Journal of Applied Physics ARTICLE scitation.org/journal/jap

Study of underwater discharge initiated by a high-voltage preliminary pulse produced by a Marx generator

Cite as: J. Appl. Phys. **133**, 033301 (2023); doi: 10.1063/5.0132851
Submitted: 31 October 2022 · Accepted: 2 January 2023 ·
Published Online: 19 January 2023

Vitaliy Stelmashuk,[1,a)] Andrii Tuholukov,[1] Yakov E. Krasik,[2] Petr Hoffer,[1] Jiri Schmidt,[1] Jaroslav Straus,[1] and Alexandr Frolov[1]

AFFILIATIONS

[1]Department of Pulse Plasma Systems, Institute of Plasma Physics of the Czech Academy of Sciences, Prague, Czech Republic
[2]Physics Department, Technion, Haifa 320003, Israel

[a)]**Author to whom correspondence should be addressed:** stelmashuk@ipp.cas.cz

ABSTRACT

The results of experimental research on the acoustic and electrical characteristics of underwater spark discharges facilitated by a preliminary discharge are presented. The latter was produced through the application of a short duration high-voltage pulse formed by a Marx generator. The application of this pulse lead to the formation of a low-density region in the form of a streamer which transformed to an oscillating vapor cavity. It was shown that this method provided a breakdown of a significantly increased interelectrode gap for the same charging voltage of the main capacitor and allowed the generation of stronger shocks. The temporal development of transient discharges in a long gap and the relationships between the hydrodynamic and electrical parameters of such discharges are reported and analyzed.

I. INTRODUCTION

The generation of shocks by underwater electrical discharges has attracted significant interest because of their practical applications in medicine[1]; oil and gas technology for well stimulation[2,3]; and electrical discharge machining.[4] A detailed study of the optimization of shock generation is of particular interest. The shock amplitude depends on the deposited energy, energy density, and energy density rate deposition in the discharge[5–7] which depend on pulse power source parameters such as the capacitance of capacitors, their charging voltage, and the discharge circuit inductance. Also, the shock amplitude depends on the efficiency of the electrical energy transfer to the acoustical energy of underwater spark expansion. The efficiency of electrical energy transfer to the acoustical energy is determined by the characteristic impedance mismatch between the pulse power source and the resistance of the spark channel. As a rule, the characteristic impedance of the pulse power source exceeds spark resistance. This results in dumped current oscillation and, respectively, a slower energy deposition into the spark channel and a reduced pressure of the generated shock.[6]

The impedance mismatch can be improved by increasing the interelectrode gap, which increases spark channel resistance.[6] However, the increase of an interelectrode gap also results in a deterioration of breakdown conditions and an inability of the underwater spark generation. A physical property can be used to facilitate the electrical breakdown process: a typical order of the electrical breakdown field in air at normal pressure is 30 kV cm^{-1} which is over ten times smaller than the electrical field required for the breakdown in water. The gas bubble injected between the electrodes reduces the electric field required for the electrical breakdown.[8] Two methods of underwater discharge inception using gas bubble generation have been proposed by the author: by a shock[9–12] and by direct gas injection into the interelectrode space.[13] Besides, it should be mentioned that the breakdown threshold can be reduced using electrolysis.[14,15] The first and the third methods consist in the generation of a number of microbubbles between the electrodes; the second method employs a single gas bubble creation on the electrode surface. Each method has advantages and disadvantages to consider. The main disadvantage of the method utilizing a shock wave is its high cost (two pulse high-voltage generators are necessary) and bulkiness of the experimental setup.[9–12] The main advantages include high precision on time triggering and independence of the mechanical parameters

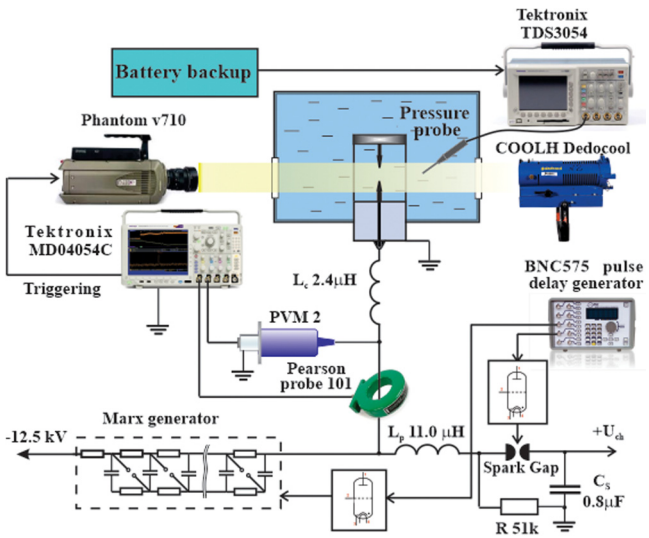

FIG. 1. Schematic diagram of the experimental setup.

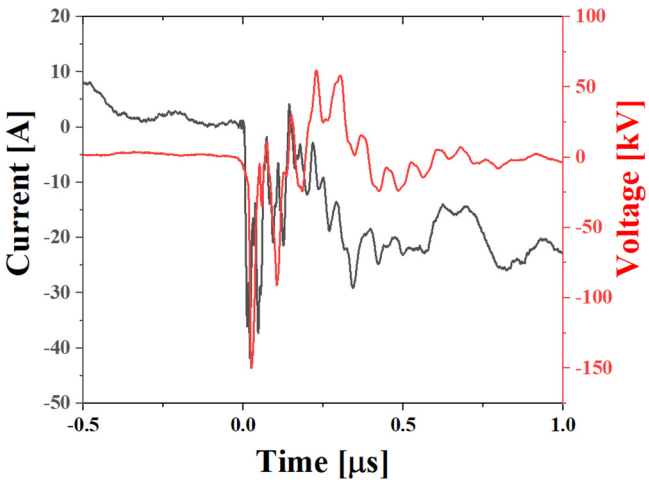

FIG. 2. Typical current and voltage waveforms of the preliminary pulse generated by the Marx generator.

of the electrode system. The benefit of the method using a gas bubble injection[13] is its low cost. Its major disadvantage is the substantial jitter of bubble injection explained by water penetration into the outlet hole. The use of water electrolysis is a low-cost method.[14,15] The effect of buoyancy makes this method sensitive to the electrode system orientation and can potentially limit the potential use. Generally, an amplitude of a shock wave depends on the energy deposited to the discharge and generally not on the discharge inception, with the exception of the bubble injection method. It was found that a shock wave magnitude strongly depends on the bubble size.[16]

In this study, a new method of underwater discharge stimulation using a low inductance, compact Marx generator is presented. The application of a preliminary high-voltage (HV) pulse generated by the Marx generator on the anode creates favorable conditions for an electrical breakdown in the pin-to-pin electrode system. The compact Marx generator used for preliminary pulse generation is relatively cheap and provides precise triggering timing. In the case of discharge generation in the plate-to-plate electrode system, where the energy of the preliminary pulse has to be increased, the cost of such a Max generator would substantially increase.

II. EXPERIMENTAL SETUP

The experimental setup is shown in Fig. 1. A pin-to-pin electrode system was mounted into a tank filled with tap water (conductivity of ~400 μS cm^{-1}). The tungsten made anode had a diameter of 1.6 mm sharpened at its top to a radius of ~0.1 mm. After ~30 experiments, the anode curvature radius increased to 0.25 mm. The brass cathode was 6 mm in diameter, sharpened at the top to a radius of 0.25 mm, which increased to 0.4 mm after ~30 experiments and did not significantly change after that. The typical anode–cathode interelectrode distances were 10 and 15 mm. The preliminary discharge was generated through the application of a negative HV pulse produced by a Marx generator having 12 stages; each stage was of 1 nF capacitor charged to 12.5 kV (see Fig. 1). The main pulse power source (PPS) consisted of a capacitor bank C_s and an inductance coil L_c. The capacitor C_s (0.8 μF) was charged up to 13 kV. These charging voltages did not lead to the interelectrode gap breakdown without the assistance of the preliminary discharge initiation by the negative HV pulse produced by the Marx generator. A triggered spark gap switched the capacitor C_s with an adjustable delay controlled by the BNC 575 pulse generator in the range of 0–100 μs with respect to the beginning of the application of the Marx generator HV pulse.

Because of the large differences in amplitudes and in the timescales of the preliminary and main HV pulses, different probes

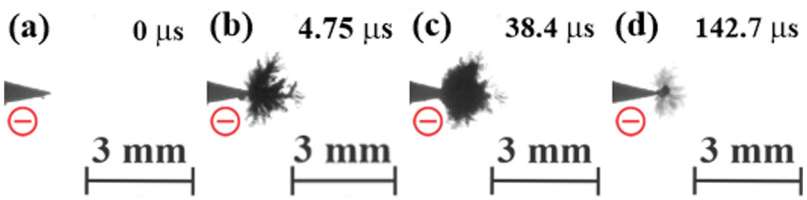

FIG. 3. Shadowgraph visualization of a negative streamer and the dynamics of a cavitation bubble generated by a Marx generator (d = 15 mm) taken at different times after triggering the discharge: (a) 0 μs; (b) 4.75 μs; (c) 38.4 μs; (d) 142.7 μs. The polarity of the preliminary pulse is the opposite of the polarity of the main discharge.

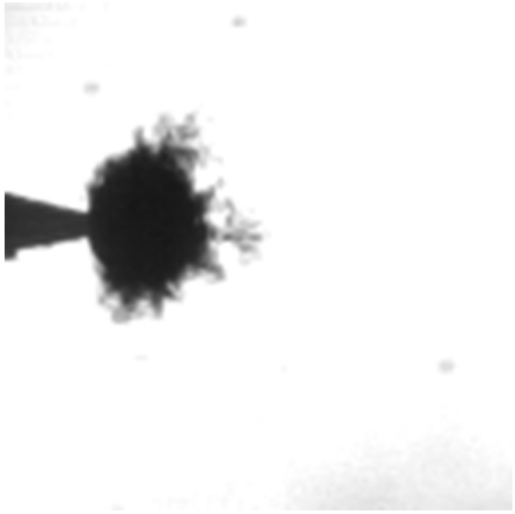

FIG. 4. Experimental video of a negative streamer and the dynamics of a cavitation bubble generated by a Marx generator ($d = 15$ mm). Multimedia view: https://doi.org/10.1063/5.0132851.1

were used to measure the voltage and current waveforms of the preliminary and main discharge pulses. A custom-made calibrated D-dot sensor (not shown in Fig. 1) mounted in the vicinity of the electrode system was used to measure the Marx generator HV pulse and a current sensor with a diameter of 10 mm[16] (not shown in Fig. 1) was used for current measurements. The measured data from the sensors were numerically integrated; the resulting Marx voltage and current waveforms are shown in Fig. 2.

The voltage and current waveforms of the main discharge are measured by the voltage divider PVM-4 2000:1 (North Star Research Co.) and the Pearson probe (model 101), respectively, and are recorded with an oscilloscope (Tektronix MDO 4054C). The inductive coil L_P (~11 μH) (Fig. 1) protects the capacitor C_s from the HV pulse generated by the Marx generator. L_c (~2.4 μH) designated the inductance of the HV cable connecting an electrode system with the PPS. The current sensor-produced signal served as the trigger source of the oscilloscope. The oscilloscope generated the output trigger signal that switched the high-speed camera Phantom v710, equipped with a Nikon 200 mm f/4D IF-ED AF micro objective. The time interval between the camera frames was 4.75 μs and the frame exposure was 0.68 μs. The discharge processes were visualized using the shadowgraph method. The backlight source was a COOLH Dedocool tungsten light head. The spark discharge was accompanied by the generation of shock whose time of flight and intensity were measured using a Müller-plate needle hydrophone (bandwidth of 0.3–11 MHz). As a sensitive element for measuring pressure, the tip hydrophone was placed at 90 mm from the electrode gap.

A streamer growth velocity function was measured using high-speed camera recordings. The average streamer velocity V_{i+1} attained in the time period between frames i and $i+1$ is calculated as a difference of streamer length observed on two adjacent frames divided by a period T_f between them,

$$V_{i+1} = \frac{L_{i+1} - L_i}{T_f}, \tag{1}$$

where L_i and L_{i+1} are the streamer lengths determined from frames i and $i+1$, respectively.

III. EXPERIMENTAL RESULTS

Figure 3 shows the shadow images of the underwater discharge induced by the preliminary HV pulse application. The full video sequence of the dynamic evolution of the electrical discharge with subsequent bubble oscillation can be found in Fig. 4. The branched negative streamer was characterized by a bush-like structure consisting of a number of filaments developing around the electrode tip, which is typical for a cathode-initiated discharge.[17] The duration of the streamer growth is correlated with the duration of the preliminary HV pulse (~50 ns) (Fig. 2) which is much shorter than the time interval between the video frames (4.74 μs). Therefore, the time and space evolution of the negative streamer could not be captured by the camera. After the streamer growth stopped, the filaments started to thicken, and the branched streamer gradually transformed into the vapor cavity [Figs. 3(b), 3(c), and 4]. When the cavity reaches its maximum size, it starts to collapse [Fig. 3(d)], then rebound and oscillates (Fig. 4) with a period of ~90 μs. The cavitation is accompanied by the disintegration of oscillating bubbles, and a cloud of long-lived microbubbles is formed [Figs. 3(d) and 4]. The sustained presence of the oscillating cavity during hundreds of microseconds, and/or a vast number of microbubbles persisting in the area for several milliseconds created favorable conditions for the electrical breakdown independently of the time delay τ_d between the preliminary pulse and the main discharge. The delay τ_d varied up to 100 μs but no difference in breakdown parameters and dynamic of discharge evolution was observed. Obviously, it can be explained by the fact that the dimension of a streamer generated by a Marx generator, the subsequent cavitation bubble, and the cloud of microbubbles are small compared with the interelectrode distance.

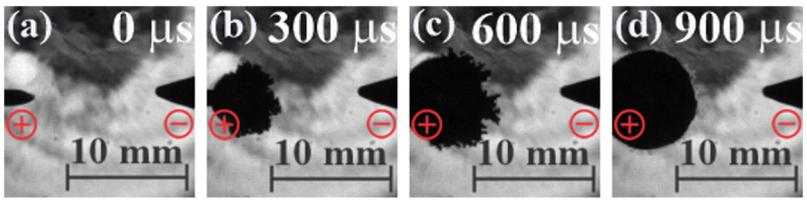

FIG. 5. Shadowgraph images of the discharge obtained without the application of the preliminary high-voltage pulse ($U_{ch} = 10$ kV, $d = 10$ mm) taken at different times after triggering the discharge: (a) 0 μs; (b) 300 μs; (c) 600 μs; and(d) 900 μs.

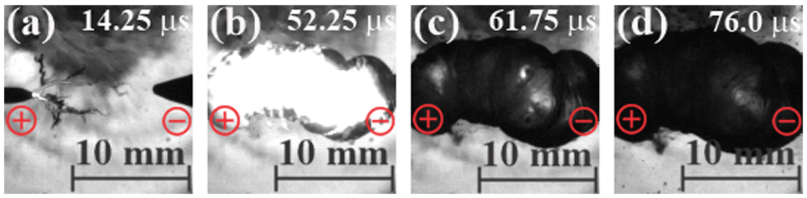

FIG. 6. Shadowgraph images of the spark discharge generated with a preliminary pulse (U_{ch} = 10 kV, d = 10 mm, τ_d = 0 s) taken at different times after triggering the discharge: (a) 14.25 μs; (b) 52.25 μs; (c) 61.75 μs; and (d) 76.0 μs.

The main experimental parameters which determined the discharge process were (a) the interelectrode distance d; (b) the charging voltage U_{ch} of the capacitor C_s; (c) the voltage U_b at the moment of breakdown; (d) the maximal electrical energy deposited to the discharge: $E_{sp} \leq 0.5C_s \times U_b^2$; and (e) the impedance of the PPS: $Z_{pps} = \sqrt{(L_C + L_p)/C_s}$.

The time evolution of the discharge generated without a preliminary HV pulse at $d = 10$ mm and $U_{ch} = 10$ kV is shown in Fig. 5. The electric field in the vicinity of the anode was not sufficient to initiate the electrical breakdown and only a corona-like discharge was formed which later transformed into an oscillating bubble.[18] The current and voltage waveforms decreased exponentially, similar to the results obtained in Ref.[18].

For the same experimental conditions ($d = 10$ mm and $U_{ch} = 10$ kV), the application of the preliminary pulse facilitated the breakdown in 50% of discharges. Shadowgraph images of the discharge development and current and voltage waveforms are shown in Figs. 6–8, respectively. A fast decaying current and voltage oscillations indicated that the underdamped discharge was realized. The preliminary HV pulse facilitated to form a branched streamer [Fig. 6(a)], in contrast to the bush-like corona obtained without the application of the preliminary HV pulse [Fig. 5(b)]. When the streamer reached the cathode, the breakdown occurred, and the underwater spark was generated. The high-speed camera frames are overexposed during 38 μs after the gap breakdown (Fig. 7). The first observable frame in Fig. 6(b) demonstrates a slightly kinked spark channel emitting an intense light whose intensity decreases with the spark expansion [Fig. 6(c), also Fig. 7] and the spark gradually transforms into an expanding vapor cavity [Fig. 6(d)].

An increase of the charging voltage to $U_{ch} = 13$ kV, for the same $d = 10$ mm and without the application of a preliminary HV pulse, resulted in a reliable electrical breakdown. The images shown in Fig. 9 (and also Fig. 10) represent the temporal development of the discharge with current and voltage waveforms presented in Fig. 11. Image (a) in Fig. 9 shows the branched streamer growing from the anode. The temporal development of the discharge is similar to that described above (see Figs. 9 and 10).

The increase of the interelectrode distance up to 15 mm led to an increase of the spark resistance which approached the PPS impedance.[6] The application of the preliminary HV pulse facilitated the breakdown with a 20% probability. Figure 12 (and also Fig. 13) shows a set of images of the discharge correlated with the waveforms in Fig. 14 when the spark gap is triggered at $\tau_d = 67$ μs. The image Fig. 12(a) shows the negative streamer initiated by the preliminary HV pulse (the magnified images of a similar streamer and the cavity into which it transformed are shown in Fig. 3).

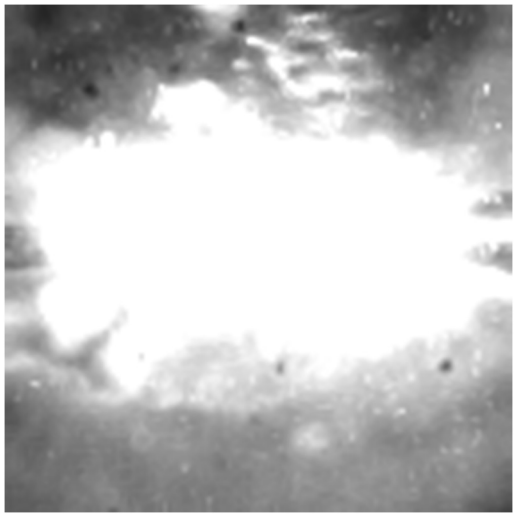

FIG. 7. Experimental video of the spark discharge generated with a preliminary pulse (U_{ch} = 10 kV, d = 10 mm, τ_d = 0 s). Multimedia view: https://doi.org/10.1063/5.0132851.2

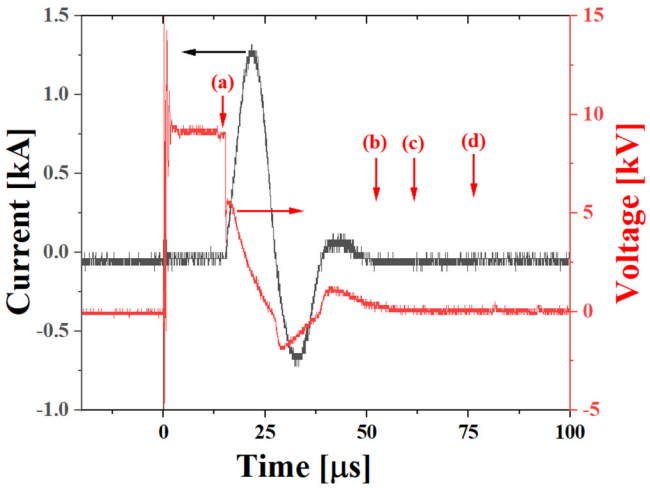

FIG. 8. Current (black) and voltage (red) waveforms of the discharge generated with the preliminary pulse (U_{ch} = 10 kV, d = 10 mm, τ_d = 0 s). The labels in the figure correspond to the images in Fig. 6.

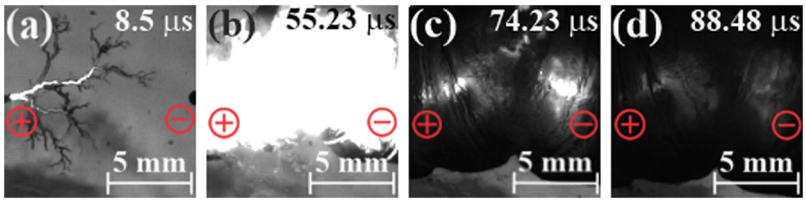

FIG. 9. Shadowgraph images of the spark discharge generated without the preliminary pulse (U_{ch} = 13 kV; d = 10 mm) taken at different times after triggering the discharge: (a) 8.5 μs; (b) 55.23 μs; (c) 38.4 μs; (d) 142.7 μs.

During the first 67 μs following the application of the preliminary HV pulse, the cavity reached a diameter of ~1.5 mm (Fig. 13) and the main discharge is incepted. The branched streamer growing from the cavity is visible in the image in Fig. 12(b). One of the branches becomes brighter, accelerates toward the cathode, bridges the electrode gap [Figs. 12(c) and 13], and finally, the breakdown occurs. The expanding spark channel reproduces a curvature of the main streamer branch [Fig. 12(d)] and maintains this form after its transformation into the vapor cavity [Figs. 12(e) and 12(f)]. The voltage and current waveforms shown in Fig. 14 exhibit an absence of oscillations. The absence of oscillations could be related to the low residual voltage remaining in the capacitor C_s (Fig. 10) whose value of −1.7 kV is not sufficient to sustain the discharge in the channel under high-pressure conditions typical for underwater sparks.[19]

The decrease of U_{ch} from 10.5 kV down to 10 kV at the same interelectrode distance of 15 mm did not affect the breakdown probability but substantially changed the discharge development. Images of the discharge evolution are shown in Fig. 15 (and also Fig. 16) with the current and voltage waveforms shown in Fig. 17.

Qualitatively, the evolution of the breakdown can be described as follows. At the beginning of the pre-breakdown phase, the initial dark filaments of 0.2–0.4 mm in diameter (Fig. 16) are developed. After that, the luminous leader streamer growing from one of the branches is formed [Figs. 15(a) and 16]. In contrast to the streamers observed in the images in Figs. 6(a), 9(a), 12(b), and 12(c), the streamer shown in Figs. 15(a)–15(c) has a smaller number of branches, thicker roots, and its morphology is similar to that of a cathode-initiated streamer in transformer oil.[17] The growth path of the streamer was close to a twisted arc. The streamer propagation velocity significantly drops in 22 microseconds (Fig. 18). The deceleration of the streamer is accompanied by its transformation into an irregular vapor cavity characterized by low radial expansion [Figs. 15(b), 15(c), and 16]. When the edge of it finally grew close enough to the cathode, the conditions for strong local electric field enhancement were achieved on this edge and the processes of field-induced dissociation and ionization of molecules were initiated. The vapor cavity transforms back to the rapidly growing streamer and the breakdown finally occurs [Figs. 15(d) and 16]. The spark channel radially expanded, keeping the curvature of the streamer. After the current termination, the spark gradually transformed into an expanding vapor cavity. The capacitor C_s was not fully discharged, and the residual voltage of −2.4 kV remained. However, the discharge of the capacitor through the high-pressure cavity channel was infeasible which led to plasma quenching. Later, the pressure inside the cavity steadily decreased with the cavity expansion and the capacitor C_s slowly discharged through water

FIG. 10. Experimental video of the spark discharge generated without the preliminary pulse (U_{ch} = 13 kV; d = 10 mm). Multimedia view: https://doi.org/10.1063/5.0132851.3

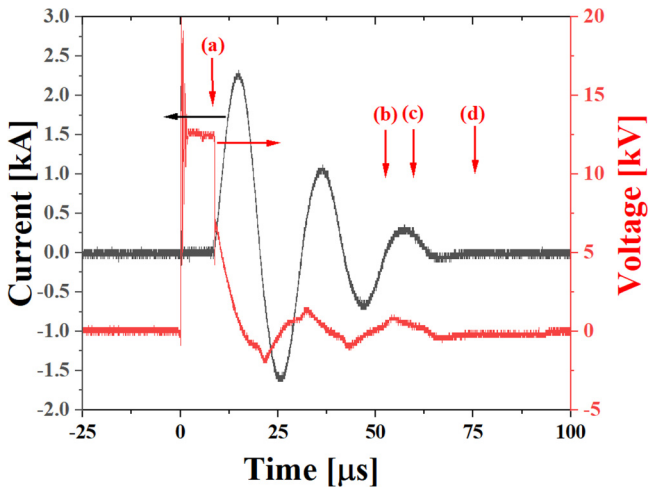

FIG. 11. Current (black) and voltage (red) waveforms of the discharge generated without a preliminary pulse (U_{ch} = 13 kV, d = 10 mm). The labels in the figure correspond to the images in Fig. 9.

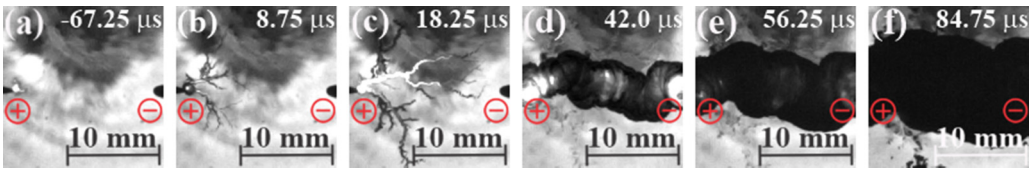

FIG. 12. Shadowgraph images of the spark discharge generated with a preliminary pulse (U_{ch} = 11 kV, d = 15 mm, τ_d = 67 μs) taken at different times before and after triggering the discharge: (a) −67.25 μs; (b) 8.75 μs; (c) 18.25 μs; (d) 42.0 μs; (e) 56.25 μs; and (f) 84.75 μs.

remaining in contact with the electrodes. In 495 μs following discharge initiation, the residual voltage in the capacitor C_s was 1.1 kV and the pressure in the channel dropped low enough for the current re-strike to be initiated. The dim light emission near the cathode can be discerned in Figs. 15(f) and 16. This re-strike is accompanied by transient current and voltage fluctuations detected after 500 μs (see Fig. 17).

IV. DISCUSSION

In Sec. III, it was shown that the application of the preliminary HV facilitated a breakdown process by forming low-density locations in water, first in the form of a streamer which transferred to a cavity, and the latter which disintegrated into a cloud of microbubbles. The latter allowed electron avalanching and the formation of streamers in these locations in a relatively low applied electric field, thus developing the main breakdown.[8,18,20] The streamer propagation could be explained by ionization processes,[18,19,21] namely, the evaporation of water in the vicinity of the streamer tip.[17] However, a positive feedback between the charge generation and the locally induced electric field at the tip had to be excluded because the measured streamer velocity is subsonic (see Fig. 13). The comparison of the results presented in Fig. 18 and Table I shows that the streamer velocity correlates with the U_b value, which determines the electric field at the streamer tip. A minor exception was observed in the case of the streamer depicted by a cyan curve. Despite having the lowest U_b, the streamer velocity slightly exceeded the velocities depicted by black and green curves during the first 15 μs after the discharge initiation. This apparent contradiction could be related to the streamer's different morphology. The branching of streamers shown in Figs. 6(a), 9(a), 12(b), and 12(c), leads to current and subsequent charge redistribution between multiple pathways.[17] The streamers shown in Figs. 15(a) and 5(b) are less branched, and accordingly, could carry a larger charge in the main branch and a subsequent increase of velocity. The latter led to the enhancement of the electric field at the tip of the streamer and, respectively, an increase in its velocity. Nevertheless, 20 μs after the main discharge initiation, the streamer transformed into the vapor cavity, the above-mentioned mechanism of streamer propagation did not play any role, and the cavity expansion was caused by overpressure.

Figure 19 shows the measured acoustic waveforms with the shock pressure amplitudes P_{sw} presented in Table I. The "piston" effect of the spark channel expansion resulted in pressure exertion on the surrounding water during the acceleration phase of the

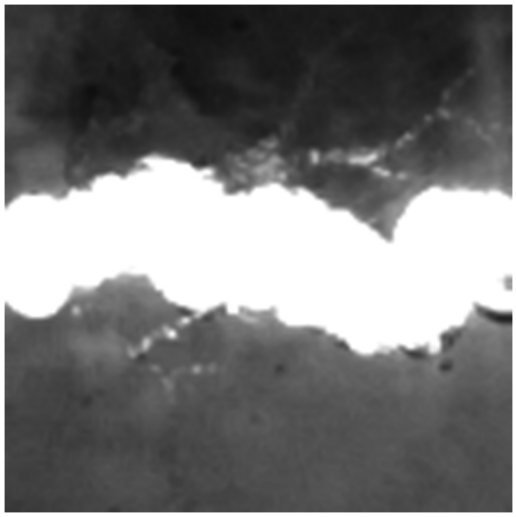

FIG. 13. Experimental video of the spark discharge generated with a preliminary pulse (U_{ch} = 11 kV, d = 15 mm, τ_d = 67 μs). Multimedia view: https://doi.org/10.1063/5.0132851.4

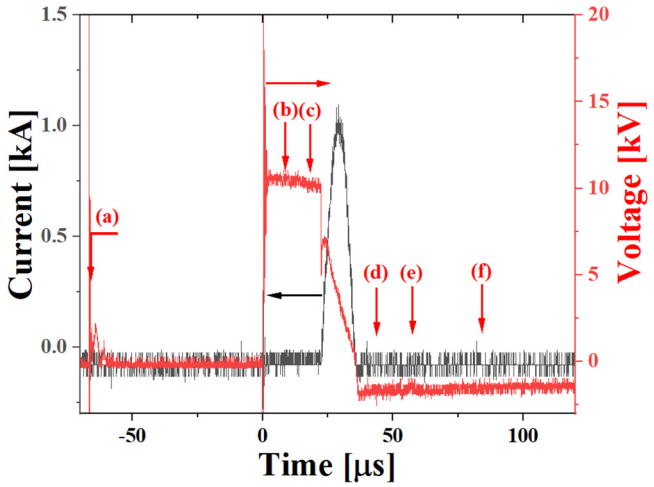

FIG. 14. Current (black) and voltage (red) waveforms of spark discharge generated with a preliminary pulse (U_{ch} = 11 kV, d = 15 mm, τ_d = 67 μs). The labels in the figure correspond to the images in Fig. 12.

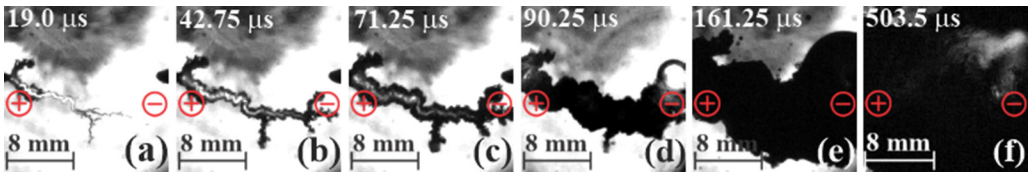

FIG. 15. Experimental video of the spark discharge generated with a preliminary pulse (U_{ch} = 10 kV, d = 15 mm, τ_d = 0 s) taken at different times after triggering the discharge: (a) 19.0 ms; (b) 42.75 ms; (c) 71.25 ms; (d) 90.25 ms; (e) 161.25 ms; and (f) 503.5 ms.

FIG. 16. Shadowgraph images of the spark discharge generated with a preliminary pulse (U_{ch} = 10 kV, d = 15 mm, τ_d = 0 s). Multimedia view: https://doi.org/10.1063/5.0132851.5

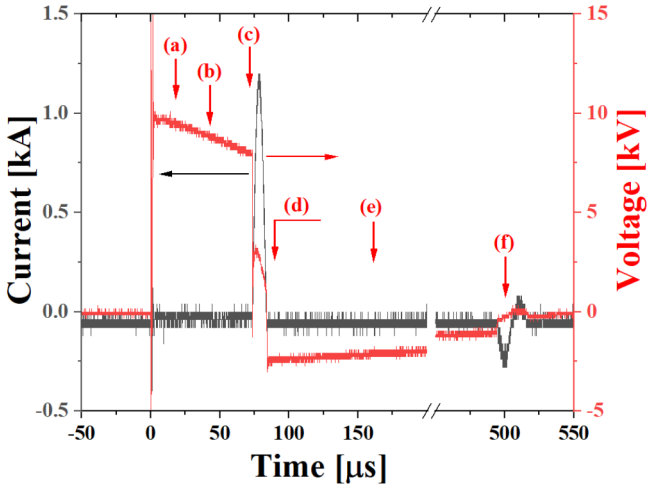

FIG. 17. Current (black) and voltage (red) waveforms of the spark discharge generated with a preliminary pulse (U_{ch} = 10 kV, d = 15 mm, τ_d = 0 μs). The labels in the figure correspond to the images in Fig. 15.

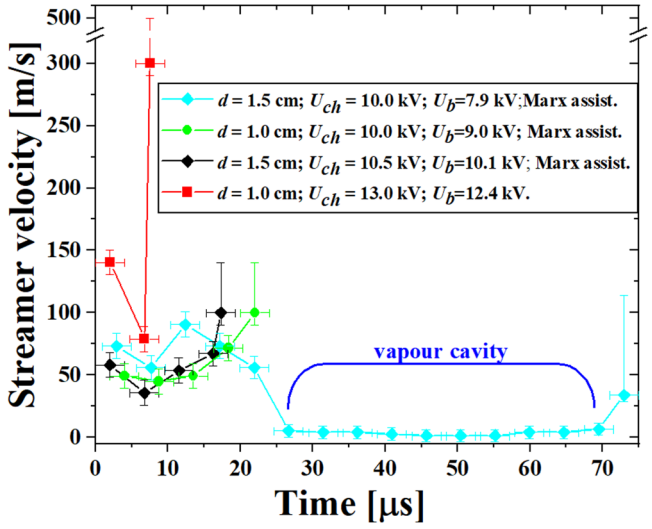

FIG. 18. Streamer velocities vs time for different discharge conditions.

expansion which led to a shock generation.[19,22–25] The shock pressure strongly depended on the total energy deposited into the spark during the acceleration phase. Therefore, instead of using the full energy deposited to the spark $E_{sp} = C^* U_{br}^2/2$ (where C is the capacitance of C_s and U_{br} is the voltage across the capacitor C_s at the moment of the electrical breakdown) as a parameter specifying the efficiency of shock generation, it was more relevant to consider the electric energy $E_{ac} = \int_{t_0}^{t_{Pmax}} i(t)u(t)dt$, where t_{Pmax} is the time corresponding to the maximum electric power dissipated in the spark. In the papers of Refs. 22 and 23 which focus on the generation of short sparks, the upper integration limit was defined as a time of maximum velocity of the spark expansion and was measured using a high-speed camera. In the case of the long sparks described in this paper, our diagnostics were not sufficient for such a task. Here, we operated under the assumption that the acceleration of spark expansion was proceeding while the electrical power was increasing. Let us note that the calculated energy E_{ac} could not be considered as equivalent to the acoustic energy of the shock, nor to the mechanical energy of spark expansion.

The power function was calculated as a product of the experimentally measured voltage and current $u(t)$ $i(t)$. The image in Fig. 20(a) shows power waveforms with marked t_{Pmax} and Table I and Fig. 19 present the shock pressures P_{sw}. There is a good

TABLE I. Electrical and hydrodynamic parameters of spark discharges.

D (mm)	Marx generator	U_{ch} (kV)	U_b (Kv)	E_{sp} (J)	E_{ac} (J)	P_{sw} (MPa)
10	No	13.0	12.4	60.5	11.6	3.6
	Yes	10.0	9.0	32.4	8.8	2.7
15	Yes	10.0	7.9	25.0	8.8	<0.1
	Yes	10.5	10.0	40.0	13.5	5.2

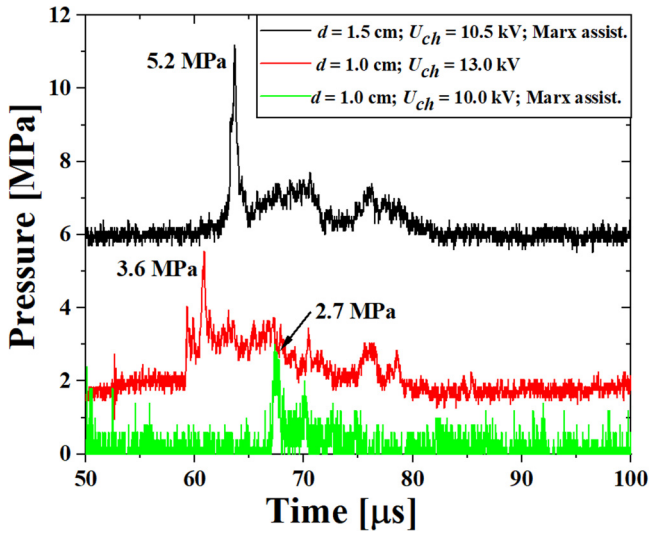

FIG. 19. Acoustic waveforms.

correspondence between the energies E_{ac} and shock amplitudes P_{sw} obtained at different experimental conditions (see Table I) for discharges depicted by black, red, and green curves in Figs. 19 and 20. The discharge presented in Figs. 15–17 with the power depicted by the cyan curve [Fig. 20(a)] presents a special case. The power curve was identical to the green curve and the energies E_{ac} were expectedly equal, although the pressures of the corresponding shocks were significantly different (see Table I). A possible explanation lies in the different streamer morphology just before the breakdown. Figure 16 demonstrates a substantial decline in streamer growth velocity and its light emission. Also, the velocities of radial expansion and propagations become similar just before the breakdown. The preliminary breakdown streamer [see Fig. 15(c)] could, therefore, be considered as a long vapor cavity. In our recent research[26] on discharges in water with gas bubbles, we found that the pressure of a shock wave generated by this type of discharge substantially decreased with the increase of the injected bubble volume.[26] A possible explanation is that a spark channel expansion in the cavity surrounded by a liquid significantly differed from a breakdown in the liquid because of different acoustical impedances of gas/vapor and liquid. The breakdown in the bubble significantly reduces the amplitude of shock pressure.[26] Further investigation is necessary.

As mentioned above and noted in Ref.,[6] an increase of the interelectrode gap up to 1.5 cm results in an increase of spark resistance, which becomes almost equal to the PPS impedance of 4.1 Ω [depicted by a dashed blue line in Fig. 20(b)]. The significance of impedance matching is confirmed by a comparison of the shock pressures presented in Table I with the resistance of sparks calculated for the first half period of current oscillations [see Fig. 20(b)]. The resistance was calculated as a divide of the experimentally measured voltage and the current $u(t)$ $i(t)$. In case of a discharge, when shock pressures reach 5.2 MPa, as depicted by the black curves in

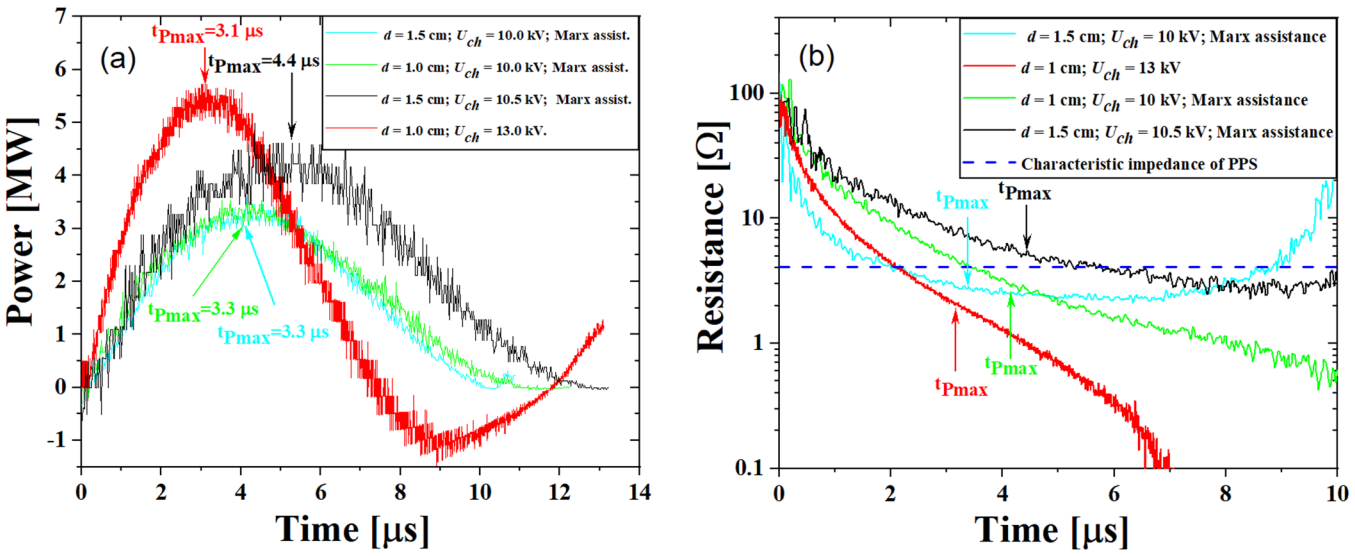

FIG. 20. Calculated power (a) and resistances (b) of the spark channel. Zero time corresponds to a moment when a streamer intersects an interelectrode gap.

Figs. 19 and 20(b), the spark resistance slowly approaches the PPS impedance depicted by the dashed blue line and becomes almost close to this value at a moment of maximum electric power dissipated in the spark. The red curves in Figs. 19 and 20(b) depict the dynamic resistance when a shock with a 3.6 MPa pressure is registered. In this case, the spark resistance decreased very rapidly and became smaller than the PPS impedance after 2.2 μs. One can suppose that in this case, the time evolution of the spark resistance determined the efficiency of the shock generation more effectively than the electrical power. The resistances of the other two discharges differ from each other despite their identical power deposition [see Fig. 20(a)] and equal energies E_{ac} (see Table I). In general, one can conclude that the shock pressure depends on the energy density and the matching between the spark resistance and the PPS impedance.

V. CONCLUSIONS

This study presents the results of the generation of an electrical discharge facilitated by the application of a preliminary HV pulse produced by a Marx generator. The discharge formed by this preliminary HV pulse created a vapor cavity and a cloud of microbubbles inside the interelectrode gap. It has been shown that these low-density regions favor the electrical breakdown of long interelectrode gaps. The main advantage of a longer gap breakdown is an increase of the spark resistance. It has been found that when an optimal electrical energy deposition occurs and a maximum shock is generated, a temporal spark resistance slowly approaches the PPS impedance.

ACKNOWLEDGMENTS

This work was conducted under sponsorships and with the support of the Czech Science Foundation (Grant No. GA18-12386S) and the Ministry of Education, Youth and Sports of the Czech Republic (INTER-EXCELLENCE/Inter-Cost LTC20061).

AUTHOR DECLARATIONS

Conflict of interest

The authors have no conflicts to disclose.

Author Contributions

Vitaliy Stelmashuk: Conceptualization (equal); Data curation (equal); Formal analysis (lead); Funding acquisition (lead); Investigation (lead); Methodology (lead); Project administration (lead); Resources (lead); Supervision (lead); Validation (lead); Visualization (lead); Writing – original draft (lead); Writing – review & editing (lead). **Andrii Tuholukov:** Data curation (equal); Investigation (equal). **Yakov E. Krasik:** Conceptualization (equal); Methodology (equal); Resources (equal); Validation (equal); Writing – review & editing (equal). **Petr Hoffer:** Investigation (supporting); Methodology (supporting). **Jiri Schmidt:** Methodology (supporting); Resources (supporting); Software (supporting). **Jaroslav Straus:** Methodology (supporting); Resources (supporting). **Alexandr Frolov:** Resources (equal).

DATA AVAILABILITY

The data that support the findings of this study are available within the article.

REFERENCES

[1]P. Lukes, P. Sunka, P. Hoffer, V. Stelmashuk, P. Pouckova, M. Zadinova, J. Zeman, L. Dibdiak, H. Kolarova, K. Tomankova, S. Binder, and J. Benes, "Focused tandem shocks in water and their potential application in cancer treatment," Shock Waves **24**(1), 51–57 (2014).
[2]K. Lee, K. J. Chung, Y. S. Hwang, and C. Y. Kim, "Underwater spark discharge with long transmission line for cleaning horizontal wells," J. Appl. Phys. **121**, 243302 (2017).
[3]F. Ren, L. Ge, V. Stelmashuk, T. E. Thomas Rufford, H. Xing, and V. Rudolph, "Characterisation and evaluation of shockwave generation in water conditions for coal fracturing," J. Nat. Gas Sci. Eng. **66**, 255–264 (2019).
[4]S. Kumar, R. Singh, T. Singh, and B. Sethi, "Surface modification by electrical discharge machining: A review," J. Mater. Process. Technol. **209**(8), 3675–3687 (2009).
[5]V. Stelmashuk and P. Hoffer, "Shock waves generated by an electrical discharge on composite electrode immersed in water With different conductivities," IEEE Trans. Plasma Sci. **40**, 1907–1912 (2012).
[6]Y. Sun, I. V. Timoshkin, M. J. Given, M. P. Wilson, T. Wang, S. J. MacGregor, and N. Bonifaci, "Acoustic impulses generated by air-bubble stimulated underwater spark discharges," IEEE Trans. Dielectr. Electr. Insul. **25**, 1915–1923 (2018).
[7]S. W. Liu, L. Yi, Z. Y. Li, X. D. Li, G. Zhou, H. Li, and F. Lin, "Effect of electrical breakdown modes on shock wave intensity in water," IEEE Trans. Dielectr. Electr. Insul. **25**, 1679–1687 (2018).
[8]S. M. Korobeinikov, A. V. Melekhov, and A. S. Besov, "Breakdown initiation in water with the aid of bubbles," High Temp. **40**, 652–659 (2002).
[9]V. Stelmashuk, "Observation of a spark channel generated in water with shock wave assistance in plate-to-plate electrode configuration," Phys. Plasmas **21**, 010703 (2014).
[10]V. Stelmashuk, "Time-resolved processes in a pulsed electrical discharge in water generated with shock wave assistance in a plate-to-plate configuration," J. Phys. D: Appl. Phys. **47**, 495204 (2014). (7 pp).
[11]V. Stelmashuk, "Time evolution of a high-voltage discharge in water With shock wave assistance in a Pin to Pin geometry," IEEE Trans. Plasma Sci. **42**, 2614–2615 (2014).
[12]V. Stelmashuk, "Time evolution of a high-voltage discharge in water With shock wave assistance in a plate-to-plate geometry," IEEE Trans. Plasma Sci. **42**, 2626–2627 (2014).
[13]V. Stelmashuk, "Microsecond electrical discharge in water in plate-to-plate configuration with nitrogen bubble injection," IEEE Trans. Plasma Sci. **44**, 702–707 (2016).
[14]K. Lee, K. Chung, and Y. S. Hwang, "Enhanced shock wave generation via pre-breakdown acceleration using water electrolysis in negative streamer pulsed spark discharges," Appl. Phys. Lett. **112**, 134101 (2018).
[15]H. Ham and J. J. Yoh, "Electronegative microchannel guided streamer propagation for in-liquid spark breakdown applications," Appl. Phys. Lett. **118**, 103905 (2021).
[16]A. P. J. van Deursen and V. Stelmashuk, "Inductive sensor for lightning current measurement, fitted in aircraft windows - part I: Analysis for a circular window," IEEE Sens. J. **11**, 199–204 (2011).
[17]R. P. Joshi, J. F. Kolb, S. Xiao, and K. H. Schoenbach, "Aspects of plasma in water: Streamer physics and applications," Plasma Processes Polym. **6**, 763–777 (2009).

[18]V. Stelmashuk and J. Schmidt, "An empirical resistance equation for the modelling of corona discharge in saline water," Plasma Source Sci. Technol. **31**, 015011 (2022). (9 pp).
[19]K. A. Naugol'nykh and N. A. Roy, *Spark Discharges in Water* (Nauka, Moscow, 1971). translation: Foreign Technology Division, *Wright-Patterson AFB OH*, 1974, 1971.
[20]P. Bruggeman and C. Leys, "Non-thermal plasmas in and in contact with liquids," J. Phys. D: Appl. Phys. **42**, 053001 (2009). (28 pp).
[21]S. Gershman and A. Belkind, "Time-resolved processes in a pulsed electrical discharge in argon bubbles in water," The European Physical Journal D **60**, 661–672 (2010).
[22]V. Stelmashuk, P. Hoffer, K. Kolacek, and J. Straus, "Experimental study of spark channel expansion in water," IEEE Trans. Plasma Sci. **48**(2), 491–499 (2020).
[23]S. Lee, K. Chung, and Y. S. Hwang, "Correlation of the peak pressure generated by an underwater spark discharge with energy absorption in a spark channel," J. Korean Phys. Soc. **66**(12), 1845–1851 (2015).
[24]V. M. Kosenkov and V. M. Bychkov, "Mathematical modeling of transient processes in the discharge circuit and chamber of an electrohydraulic installation," Surf. Eng. Appl. Electrochem. **51**, 167–173 (2015).
[25]I. Timoshkin, R. Fouracre, M. Given, and S. MacGregor, "Hydrodynamic modelling of transient cavities in fluids generated by high voltage spark discharges," J. Phys. D: Appl. Phys. **39**, 4808–4817 (2006).
[26]V. Stelmashuk, V. Prukner, K. Kolacek, A. Tuholukov, P. Hoffer, J. Straus, A. Frolov, and V. Jirasek, "Optical emission spectroscopy of underwater spark generated by pulse high-voltage discharge with Gas bubble assistant," Processes **10**, 1474 (2022).